

UniReg: Foundation Model for Controllable Medical Image Registration

Zi Li¹ Jianpeng Zhang^{1,2} Tai Ma¹ Tony C. W. Mok¹ Yan-Jie Zhou^{1,2}
 Zeli Chen¹ Xianghua Ye³ Le Lu¹ Dakai Jin¹

¹ DAMO Academy, Alibaba Group

² College of Computer Science and Technology, Zhejiang University

³ The First Affiliated Hospital of College of Medicine, Zhejiang University

alisonbrielee@gmail.com

Abstract

Learning-based medical image registration has achieved performance parity with conventional methods while demonstrating a substantial advantage in computational efficiency. However, learning-based registration approaches lack generalizability across diverse clinical scenarios, requiring the laborious development of multiple isolated networks for specific registration tasks, e.g., inter-/intra-subject registration or organ-specific alignment. To overcome this limitation, we propose **UniReg**, the first interactive foundation model for medical image registration, which combines the precision advantages of task-specific learning methods with the generalization of traditional optimization methods. Our key innovation is a unified framework for diverse registration scenarios, achieved through a conditional deformation field estimation within a unified registration model. This is realized through a dynamic learning paradigm that explicitly encodes: (1) anatomical structure priors, (2) registration type constraints (inter-/intra-subject), and (3) instance-specific features, enabling the generation of scenario-optimal deformation fields. Through comprehensive experiments encompassing 90 anatomical structures at different body regions, our UniReg model demonstrates comparable performance with contemporary state-of-the-art methodologies while achieving 50% reduction in required training iterations relative to the conventional learning-based paradigm. This optimization contributes to a significant reduction in computational resources, such as training time. Code and model will be available.

1. Introduction

Establishing anatomical correspondence [30] across images is paramount for medical image analysis and its associated clinical applications, encompassing atlas-based segmenta-

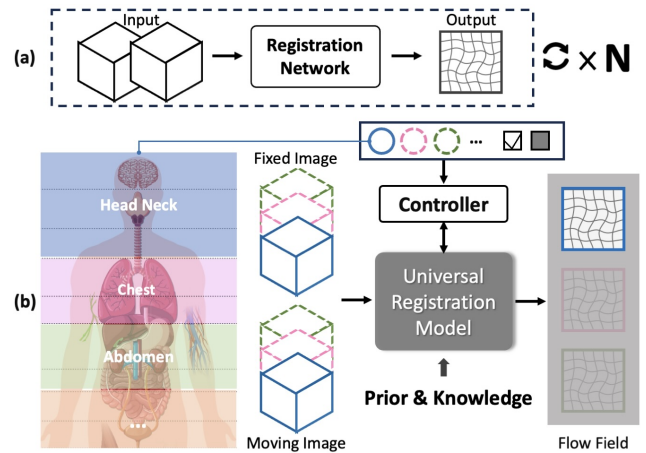


Figure 1. (a) Task-specific registration model: Conventional learning-based registration requires manual design of specialized networks for each anatomical region and registration type. This results in redundant development efforts, where N distinct tasks necessitate N training isolated models. (b) Controllable universal registration model: UniReg introduces a conditional control module that dynamically adapts to anatomical regions (circle symbols), registration types (rectangle symbols: inter-/intra-patient), and imaging characteristics. Through systematic integration of anatomical priors and knowledge within a unified architecture, the model achieves whole-body organ registration with task-aware deformation field generation.

tion [22, 51], diagnostic procedures [1, 35], and longitudinal studies [10, 40].

Conventional image registration approaches [4, 14, 39, 41, 43, 44] are often used to facilitate automatic image registration for a wide variety of registration tasks. Yet, conventional approaches are slow in practice as they rely on an iterative numerical optimization framework. These approaches estimate the optimal deformation by gradually maximizing the similarity between the target image and the transformed reference image in an iterative fashion.

Iterative optimization in conventional methods leads to a heavy computation burden, prohibiting their usage in high-throughput environments that need to process dozens to thousands of medical image scans.

More recently, learning-based registration methods [5, 6, 27, 37, 38] addressed the inefficiency of conventional methods by reformulating the iterative optimization problem to a learning problem using convolutional neural networks. Numerous studies explored advanced network architectures [29, 31, 32, 38] and implemented more efficient feature extractors [23, 25, 37] to improve registration precision.

However, due to the learning nature of these methods, the training and registration process are highly customized and task-specific, leading to inferior generalizability and flexibility compared to conventional approaches. A trivial approach to adapting a learning-based approach to multiple registration tasks is to develop multiple isolated registration networks and train them on independent task-specific datasets, as shown in Figure 1(a), which requires massive computational resources and tedious hyperparameter tuning to maximize the registration performance for each task. Alternatively, one can develop a universal registration model by training one registration network over various datasets. Yet, this approach has proved ineffective and unstable [46] as there are significant variations in the optimal set of registration hyperparameters across different image modalities, anatomical regions, and tasks. Training a typical convolutional neural network to learn multiple diverse registration tasks often results in sub-optimal registration accuracy.

In recent years, pioneering works of deformable registration [8, 17, 34] introduce a conditional image registration framework that is able to capture the effect of a wide range of regularization hyperparameters on the deformation field. While these conditional image registration frameworks offer enhanced flexibility in hyperparameter tuning, the registration network remains constrained to a single task or anatomical region.

In this paper, we present a dynamic registration paradigm for the Universal Registration model, referred to as UniReg, as depicted in Figure 1(b), representing a significant advancement towards bridging the gap between registration performance and generalization. The model comprises a shared backbone and a conditioning control mechanism. The shared backbone is dedicated to learning robust and generalized anatomical correspondences, while the conditioning control module dynamically generates optimal deformation fields for diverse scenarios, demonstrating a high level of adaptability. To initiate this conditioning control process, we encode various scenarios by integrating task-specific information, such as anatomical structures, inter- and intra-patient variations, and body parts. Furthermore, registration images are employed as a conditioning vector,

enabling the model to provide optimal solutions tailored to each registration image. We then develop a lightweight controller network that synthesizes these variable factors and encodes them into a task-specific deformation kernel, which is subsequently transmitted to the dynamic registration head to generate the deformation field.

Furthermore, our UniReg model is trained on a wide variety of scenarios and datasets, enhancing its applicability across diverse contexts and showcasing strong generalization capabilities. Moreover, we introduce specific smoothing priors and segmentation masks tailored to different tasks during training, effectively improving registration performance across various scenarios. Specifically, our dataset encompasses inter-subject registration tasks across multiple anatomical regions, including the head-neck, chest, and abdomen scanned by computed tomography (CT). It also includes two intra-subject registration tasks derived from multiphase liver CT scans and lung respiratory dynamics datasets. This extensive collection (Section 4.1) features a diverse array of 90 anatomical organs, representing nearly the entirety of the human body, from the cranial region to the pelvic area, while also incorporating tumor-affected patients (liver/lung tumors).

Empirically, UniReg exhibits performance parity with contemporary state-of-the-art registration methods while achieving a reduction of at least 50% in required training iterations relative to conventional learning-based paradigms (Section 4.4). This computational efficiency translates to a substantial decrease in resource expenditure, with training time diminished to 30–90% of that required by traditional learning methods.

The main contributions of this work are as follows:

- We propose the first controllable, unified registration framework (UniReg) that features a single network that dynamically adapts to various tasks. It eliminates the need for developing multiple task-specific registration networks, substantially reduces computational costs and lessens reliance on expertise in model development.
- We introduce a conditional control vector for universal registration that encodes anatomical structure priors, registration type constraints, and instance-specific features. A dynamic deformation generation module is further developed that facilitates adaptive registration using dynamic kernels. These components collectively provide an efficient and streamlined solution for registration tasks across diverse domains.
- We design a dynamic training strategy that leverages prior knowledge and human expertise to optimize the UniReg model. This strategy incorporates regularization priors and anatomical insights to tailor the optimization process for each specific registration task, enhancing the registration performance.
- We demonstrate that UniReg ensures flexibility and effi-

cacy in handling complex anatomical variations and registration scenarios. Our comprehensive evaluation spans a diverse array of 90 anatomical organs/tumors, representing nearly the whole human body. To the best of our knowledge, this represents the most extensive assessment in CT imaging to date.

2. Related Work

Deformable Medical Image Registration. Traditional deformable registration methods [3, 4, 14, 15, 39, 41, 44] solve an optimization problem and iteratively minimize a similarity measure, often jointly with a regularizer, to align a pair of images. Recently, learning-based deformable registration [5–7, 26, 33, 35, 37, 38], use deep networks to predict a vector field to describe the displacements directly or to estimate a velocity field from which a transformation can be obtained by integration. Compared with optimization-based approaches learning-based methods are much faster at the inference phase.

To capture large deformations, more recent methodologies underscore the importance of advancing sophisticated Convolutional Neural Networks (CNN) or Transformer architectures. These strategies [11, 27, 28, 36, 38, 52] capitalize on multi-step approaches, pyramids, cascaded structures, iterative refinement, or connecting registration to image synthesis tasks [24, 47]. Additionally, registration performance can be improved by using anatomical information during training through segmentation labels [5, 47]. Recently, SAME and SAMConvex [23, 25, 45] have investigated the utilization of pre-trained Self-supervised Anatomical embedding [49] to serve as features for registration, that contains discriminative anatomical semantic information.

However, these methods are typically optimized for specific tasks, and when they are transferred to others, the optimization or network weights must be re-executed to suit the given registration scenario.

Conditional Medical Image Registration. Conditional image registration has drawn considerable research attention in the community due to its potential in amortized hyperparameter learning [17, 34]. Mok *et al.* [34] designed a learning paradigm for conditional image registration, in which the registration network is conditioned on the dynamic regularization strength with linear modulation [18]. Hoopes *et al.* [17] propose to learn the effects of registration hyperparameters on the deformation field with Hypernetworks [13], which leverage a secondary network to generate the conditioned weights for the entire network layers. This design is more flexible than traditional convolutional networks, where the hyperparameters are fixed during the training and inference.

Apart from the image registration domain, several approaches are dedicated to enhancing the representation ca-

capacity and flexibility of segmentation networks using dynamic filters. Jia *et al.* [20] designed a dynamic filter network in which the filters are generated dynamically and conditioned on the input image. Subsequently, Zhang *et al.* [50] introduced the conditionally parameterized convolutions, which learn task-specific convolution kernels for each assigned segmentation task.

Unified Medical Image Registration. Despite a vast number of methods for deformable image registration, most of these methods are task-specific [11, 27, 38] or require manual [14, 44] or automated [17, 27, 34] hyperparameter tuning for new registration tasks.

To address this issue, some attempts have been made to explore unified medical image registration. Siebert *et al.* [42] proposed a self-configuring dual-optimization method, which amortizes the hyperparameter search using a combination of rule-based and grid search techniques. Alternatively, Hoffmann *et al.* [16] proposed a deep learning-based registration method that learns from randomly synthesized images and shapes. While learning from synthesized shapes circumvents the task-specific limitation, it lacks anatomical knowledge of the human structures, resulting in sub-optimal registration accuracy and plausibility. Subsequently, Tian *et al.* [46] collected multiple datasets from different medical domains and co-trained a unified medical image registration on them, capable of multi-task registration with a single registration network. However, it employs a uniform regularization approach that fails to incorporate essential task-specific priors and knowledge, *i.e.*, hyperparameter selection, resulting in suboptimal performance.

3. Method

Problem formulation. Let us consider n registration datasets $\{\mathcal{D}_1, \mathcal{D}_1, \dots, \mathcal{D}_n\}$ from n imaging scenarios. Here, $\mathcal{D}_i = \{\mathbf{F}_{ij}, \mathbf{M}_{ij}, \hat{\mathbf{F}}_{ij}, \hat{\mathbf{M}}_{ij}\}_{j=1}^{m_i}$ represents the i -th dataset that contains m_i image pairs. Specifically, $\mathbf{F}_{ij}, \mathbf{M}_{ij}$ are fixed and moving volumes defined over three-dimensional spatial domain $\Omega \subseteq \mathbb{R}^{D \times W \times H}$, where $W \times H$ is the spatial size of each slice and D is number of slices. The corresponding organ segmentation masks are denoted as $\hat{\mathbf{F}}_{ij}, \hat{\mathbf{M}}_{ij}$. The core of registration is a mapping function that learns a transformation to align the moving image with the fixed image space. To address the n different registration tasks, conventional solutions necessitate optimizing n registration models, with individual parameters $\theta_1, \theta_2, \dots, \theta_n$, to handle each task individually, formulated as follows:

$$\begin{cases} \min_{\theta_1} \sum_{j=1}^{m_1} \mathcal{L}_1(f_1(\mathbf{F}_{1j}, \mathbf{M}_{1j}; \theta_1), \hat{\mathbf{F}}_{1j}, \hat{\mathbf{M}}_{1j}) \\ \vdots \\ \min_{\theta_n} \sum_{j=1}^{m_n} \mathcal{L}_n(f_n(\mathbf{F}_{nj}, \mathbf{M}_{nj}; \theta_n), \hat{\mathbf{F}}_{nj}, \hat{\mathbf{M}}_{nj}) \end{cases} \quad (1)$$

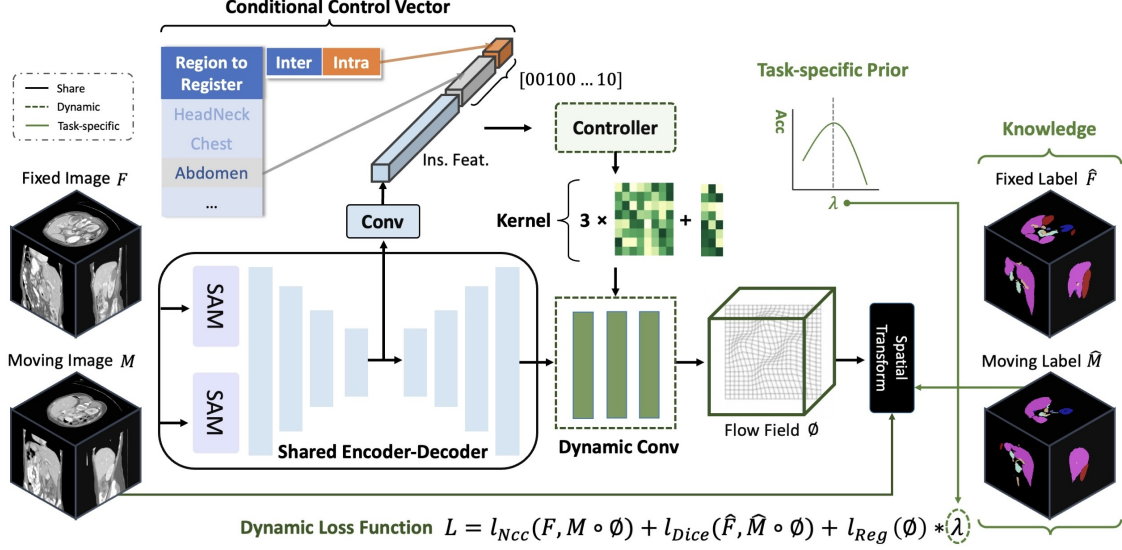


Figure 2. **Overview of the proposed universal registration model.** Our framework comprises a backbone architecture and Dynamic Registration. Leveraging our dynamic controller mechanism, we can leverage human expertise and prior knowledge of diverse registration tasks throughout the training process. At each training iteration, our framework selects task-specific hyperparameters and segmentation masks corresponding to distinct task IDs, thereby instituting optimization objectives tailored to the individual registration task.

where \mathcal{L} refers to the loss function of registration networks. In contrast, we attempt to process all registration tasks using one single network f , *i.e.* UniReg, denoted as

$$\arg \min_{\theta, \psi} \sum_i^n \sum_j^{m_i} \mathcal{L}(f(\mathbf{F}_{ij}, \mathbf{M}_{ij}; \theta, h(i; \psi)), \hat{\mathbf{F}}, \hat{\mathbf{M}}). \quad (2)$$

3.1. UniReg

We first introduce the basic structure of a UniReg in Section 3.1.1 and then describe how we define the conditioning vector in Section 3.1.2, which enables the dynamic application of UniReg to optimally estimate parameters for each registration scenario in Section 3.1.3. We elaborate on our training in Section 3.2 and detail several extra considerations during inference in Section 3.3.

3.1.1. Shared Backbone

The backbone is designed to generate feature that encompasses the semantic information of multiple organs and not constrained to a specific task. For this purpose, our unified encoder-decoder architecture is founded on the Self-supervised Anatomical embedding (SAM) [49], serving as the basic framework of our registration model, as illustrated in the left part of Figure 2. This architecture facilitates both global and local feature extraction from image pairs, shown to effectively enhance registration [23, 25, 45]. Subsequently, our encoder architecture is structured as a series of repeated residual blocks, each comprising two convolutional layers. Each convolutional layer is succeeded by an

activation function. In each downsampling phase, a convolutional operation characterized by a stride of 2 is employed, thereby reducing the resolution of the input feature maps by half. Symmetrically, the decoder progressively upsamples the feature map to enhance its resolution. At every stage, the upsampled feature map is combined with the corresponding low-level feature map from the encoder. Now, we have $\mathbf{E}_{ij} = f(\mathbf{F}_{ij}, \mathbf{M}_{ij}; \theta)$, where θ represents all backbone parameters. Here, $\mathbf{E}_{ij} \subseteq \mathbb{R}^{C \times D \times W \times H}$ and C is the channel dimension.

3.1.2. Conditional Control Vector

Our task-aware conditioning control mechanism that dynamically modulates deformation field generation through: (1) anatomical structure priors, (2) registration type constraints (inter/intra-subject), and (3) instance-specific features from images. To be specific, three hierarchical conditioning components are:

- Task activation indicator. The anatomical structure priors are encoded as an n dimensional one-hot vector as:

$$\mathbf{T}_{ik} = \begin{cases} 0, & \text{if } k \neq i \\ 1, & \text{otherwise} \end{cases} \quad k = 1, 2, \dots, n, \quad (3)$$

where $\mathbf{T}_{ik} = 1$ signifies that the registration task on k -th body part is currently being executed.

- Encoding of registration type. A embedding $\mathbf{e} \in \mathbb{R}^2$ is subsequently concatenated, formulated as:

$$\mathbf{e} = \begin{cases} [0, 1]^\top & (\text{inter-subject}) \\ [1, 0]^\top & (\text{intra-subject}) \end{cases} \quad (4)$$

This orthogonal encoding ensures disentangled learning of registration-type specific features.

- Instance-aware feature fusion: Ultimate dynamic registration results are generated through channel-wise concatenation of: image features \mathbf{E} from our backbone which is derived through mean-field inference [21] and task-conditioning vector $[\mathbf{T} \oplus \mathbf{e}]$.

3.1.3. Dynamic Deformation Generation

Inspired by adaptive architectures [20, 50], we design a task-aware dynamic network $\mathcal{G}(\cdot)$ that combines two core components: conditional filter generator and a dynamic deformation field head, as shown in the right part of Figure 2.

Instead of requiring multiple specialized or fixed networks for different tasks, our conditional filter generator produces convolutional kernels modulated by the input’s anatomical characteristics and registration task constraints. Technically, dynamic convolution kernels ω are generated through the aforementioned three components in 3.1.2. This yields:

$$\omega = \mathcal{G}([\mathbf{E}_i \oplus \mathbf{T} \oplus \mathbf{e}]) \quad (5)$$

where $\mathcal{G}(\cdot)$ is denoted as controller.

The proposed dynamic deformation field head facilitates task-specific kernel allocation across diverse registration scenarios through a parameter-efficient architecture. This module employs three cascaded $1 \times 1 \times 1$ convolutional layers and kernel parameters in three layers, denoted by $\omega = \{\omega_1, \omega_2, \omega_3\}$, are dynamically generated by the controller $\mathcal{G}(\cdot)$. Specifically, the initial two layers consist of 8 channels, while the final layer comprises 3 channels designated for estimation of deformation field $\phi \subseteq \mathbb{R}^{3 \times D \times W \times H}$. Consequently, the controller yields 171 parameters ($\#Weights : 8 * 8 * 2 + 8 * 3$; $\#Bias : 8 * 2 + 3$). Subsequently, we utilize ϕ in conjunction with a spatial transformer [19] to deform the moving image into the fixed image space.

3.2. Training

Conceptually, loss function for UniReg containing:

$$\mathcal{L} = \mathcal{L}_{Sim}(\mathbf{F}, \mathbf{M} \circ \phi) + \lambda \mathcal{L}_{Reg}(\phi) \quad (6)$$

where a similarity term \mathcal{L}_{Sim} penalizes the appearance differences. The regularizer \mathcal{L}_{Reg} promotes spatial smoothness within the transformation map. The symbol of \circ means warp operation using the spatial transformer. The λ is a trade-off hyperparameter defined based on the specific task. **Regularization prior.** Considering that the precision of the resultant transformation map is significantly affected by the selection of specific hyperparameter values [17, 27, 34] associated with the regularization in the optimization objective, we make the following efforts. we propose to pre-establish task-related hyperparameter priors $\lambda = \{\lambda_1, \lambda_2, \dots, \lambda_n\}$ using [34]. Therefore, during the

training process, the strength of regularization will be calibrated according to the task condition, ensuring the model understands the exact objectives it needs to achieve and further allowing it to handle multiple tasks.

Optional anatomical knowledge. Leveraging voxel-wise anatomical segmentation masks as spatially constrained priors, we develop an anatomy-aware multitask optimization framework that synergistically enhances UniReg’s performance across diverse registration scenarios. We integrate a multiinstitutional dataset with expert-validated annotations for 90 clinically critical anatomical structures spanning five body regions (head, neck, chest, abdomen, pelvis), implementing a dynamic supervision mechanism that selectively activates region-specific segmentation constraints.

3.3. Inference

Inference on in-distribution task. During inference, the UniReg is flexible to diverse registration tasks. Given a test image, the feature is extracted from the encoder-decoder network. Assigned with a task, the controller generates the kernels conditioned on the input image and task. The dynamic head powered by the generated kernels can automatically register the structures as specified by the task. *Inference on unseen task.* When handling unseen/out-of-distribution data, UniReg only requires the input of anatomical regions and inter/intra-properties.

4. Experiments

4.1. Dataset and Pre-processing

- *Inter-patient task on HeadNeck.* This study utilized a CT dataset¹ consisting of 240 head-neck cancer patients. The dataset includes annotations for 45 head and neck organs.
- *Inter-patient task on Chest.* A chest CT dataset [12] comprising 94 subjects was collected from hospitals. Each chest CT image features 35 manually labeled anatomical structures identified by a senior radiologist.
- *Inter-patient task on Abdomen.* The Abdomen CT dataset from Learn2Reg² includes 30 scans, each containing 13 manually labeled anatomical structures.
- *Intra-patient task on Lung.* We collected a 4D CT dataset of lungs comprising 35 patients, each featuring paired inspiratory and expiratory breath-hold images. Each image is labeled with malignancies, *i.e.* primary gross tumor volume (GTV), by a senior radiologist.
- *Intra-patient task on Liver Multiphase CT.* We gathered a multi-phase contrast-enhanced liver CT dataset of 80 tumor-diagnosed patients, with scans taken in three phases: pre-contrast, arterial, and venous. A senior radiologist annotated and verified the liver and tumor masks.

¹<https://segrap2023.grand-challenge.org/>

²<https://learn2reg.grand-challenge.org/Learn2Reg2020/>

Dataset	Task	Modality	# Label	# Train	# Val	# Test	Size	BPR Range
HeadNeck	Inter-subject	Mono	45	4446	90	841	(280, 280, 192)	0.51-1.00
Chest	Inter-subject	Mono	35	4160	90	90	(180, 180, 200)	0.31-0.84
Abdomen	Inter-subject	Mono	13	380	0	90	(250, 250, 160)	0.00-0.35
Lung GTV	Intra-subject	Mono	1	0	0	35	(256, 256, 112)	0.60-0.65
Liver	Intra-subject	Multi	2	150	10	50	(290, 290, 160)	0.33-0.53

Table 1. Data statistics of all datasets used in our experiment.

The divisions of training, validation, and testing for each registration task are summarized in Table 1, which also presents other key statistics for all datasets. To deepen the understanding of the distribution of body parts within each dataset, we include the body part regression (BPR) [48] axial ranges of the CT images. All images were adjusted to a size of $192 \times 192 \times 160$ through padding or cropping and resampled to a spacing of $2 \times 2 \times 2$ mm and oriented to the RAI direction. We aligned the inter-patient registration task datasets globally using [45].

4.2. Evaluation Metrics and Baselines

To quantify registration performance, we register each pair of images, propagate the anatomical segmentation map using the resulting transformation, and assess the segmentation overlap in the region of interest using the Dice similarity coefficient (DSC) [9]. As a negative determinant of the Jacobian at a voxel indicates local folding [2], we further compute the percentage of foldings ($\%|J_\phi| < 0$) within the deformation field to evaluate its plausibility. We also compute the standard deviation of the logarithm of the Jacobian determinant (SDlogJ) to evaluate the plausibility of deformation fields. In our experiments, SDlogJ is used for evaluating inter-subject registration, while $\%|J_\phi| < 0$ is used for assessing intra-subject registration.

We compare our method with two popular conventional registration methods (NiftyReg [44], Deeds [14]), five state-of-the-art learning-based approaches (LapIRN [38], IIRP-Net [29], CorrMLP [32], SAME [45] and uniGradICON [46]). We also compared a basic universal training approach for the SAME model: UniSAME, which uses a sequential training process, incorporating Headneck, Chest, Abdomen, and Liver datasets. We conducted training from scratch to derive the final models for the four learning-based methodologies, LapIRN, IIRP-Net, CorrMLP, and SAME. All experiments were conducted on NVIDIA Tesla V100 GPU. The commands for the four conventional methods and the remaining design choices for learning-based methods are detailed in suppl. materials.

4.3. Implementation Detail

We employ a pre-trained SAM model that produces a 128-dimensional global embedding and a local embedding for each voxel. To ensure compatibility in dimensions, we per-

form linear interpolation to resize the global feature map to match the dimensions of the local feature map. Subsequently, we apply L2 normalization to the feature embeddings. The resized global feature map is then concatenated with the local feature map and the original images along the channel dimension.

To eliminate irrelevant regions and streamline subsequent processing, we truncated the HU values in each scan to the range of $[-800, +400]$ and linearly normalized them to the range of $[-1, +1]$. The stochastic gradient descent (SGD) algorithm with a momentum of 0.99 was employed as the optimizer. The learning rate was initially set to $5e-5$, with a maximum iteration at $120k$.

4.4. Comparing to state-of-the-art methods

Inference on in-distribution task. Table 2 shows the results of the inter-subject registration on HeadNeck, Chest, Abdomen, and intra-subject registration on Liver.

1) *Achieving accuracy on par with the state-of-the-art.* Learning-based approaches yield comparable results to traditional methods and consistently outperform them across three tasks after utilizing segmentation information, highlighting the inherent advantage of deep models. However, these learning-based methods require training four distinct models for each task. In contrast, our proposed method illustrates that a single model can achieve top-tier performance - placing first or second in all four tasks - while only slightly trailing behind task-specific semi-supervised models, which are the upper bound *performance* for the single universal registration model. The qualitative assessments depicted in Figure 3 provide additional evidence of the robustness and precision of our method in aligning both the organ and tumor regions.

2) *Flexibility and versatility.* Tackling concurrently inter- and intra-subject registration tasks is hindered by the substantial disparities between these two tasks. Consequently, the existing models generally achieve satisfactory results in one category of tasks. For example, UniSAME excels in intra-registration but demonstrates suboptimal performance in inter-registration. In contrast, our method is capable of simultaneously addressing both types of tasks, even surpassing the semi-supervised SAME on Liver task.

3) *Training efficiency.* Learning-based methods generally require distinct training processes for each specific task,

Method	W/Dice	HeadNeck		Chest		Abdomen		Liver		Para. (M)	FLOPs	Train (h)
		DSC ₄₅ ↑	SDlogJ ↓	DSC ₃₅	SDlogJ	DSC ₁₃	SDlogJ	DSC ₂	% J _ϕ < 0 ↓			
Initial		41.96	0.00	45.14	0.00	32.64	0.00	78.05	0.00	—	—	—
NiftyReg [44]		52.13 [†]	0.16	51.58 [†]	0.04	34.98 [†]	0.22	81.92 [†]	0.01	—	—	—
Deeds [14]		49.87 [†]	7.18	52.72 [†]	1.28	46.52 [†]	0.44	83.50 [†]	5.81	—	—	—
LapIRN [38]		46.37 [†]	0.03	55.87 [†]	4.33	46.44 [†]	0.72	81.02 [†]	0.01	0.92	688	126
IIRP-Net [29]		51.04 [†]	1.72	54.41 [†]	3.03	52.19 [†]	5.46	82.08 [†]	0.18	0.41	242	92
CorrMLP [32]		49.05 [†]	4.87	54.40 [†]	4.42	53.03 [†]	7.28	79.91 [†]	0.29	4.19	995	896
SAME [45]		46.34 [†]	1.08	56.93 [†]	0.44	49.27 [†]	2.82	80.64 [†]	0.03	0.36	464	174
uniGrad [46]		N/A	—	47.92 [†]	—	48.30 [†]	0.31	N/A	—	—	—	—
uniSAME [45]	✓	41.58 [†]	1.15	51.48 [†]	1.80	47.09 [†]	1.43	84.23	0.21	0.36	464	176
UniReg (Ours)	✓	<u>51.44</u>	0.77	<u>61.35</u>	1.30	<u>55.56</u>	1.39	86.42	3.20	0.36	477	60
SAME* [45]	✓	52.52[†]	0.69	62.35	1.09	56.97	1.17	<u>85.30</u>	0.63	0.36	464	176

Table 2. Quantitative results of inter- and intra-subject registration between task-specific and universal models (i.e., uniGrad [46], uniSAME [45] and our UniReg). The subscript of each metric indicates the number of anatomical structures involved. †: higher is better, and ‡: lower is better. Initial: initial affine results without deformable registration. DSC results with *significant differences* ($P < 0.05$) to UniReg are highlighted with †. The best-performing results are shown in bold while the second-best results are indicated by underlining. ‘N/A’ means failed results, inferior to initial DSC. Note that SAME* represents the upper bound performance by the task-specific SAME model separately trained on each dataset using additional organ mask supervision.

Method	W/Dice	Lung GTV		Inf. (s)
		DSC ₁	% J _ϕ < 0	
Initial		67.06	—	—
NiftyReg		74.59	0.02	126.94
Deeds		81.53	0.49	134.82
LapIRN _{Chest}		N/A	—	0.18
IIRP-Net _{Chest}		N/A	—	0.17
CorrMLP _{Chest}		N/A	—	1.17
SAME _{Chest}		N/A	—	0.20
SAME* _{Chest}	✓	N/A	—	0.20
UniReg	✓	71.10	0.77	0.25
UniReg + IO	✓	73.00	0.65	4.41

Table 3. Quantitative results on unseen task. ‘N/A’ means failed results, inferior to initial DSC.

typically involving 80k optimization iterations per task. For four tasks examined in this study, this translates to a total of 320k iterations. In contrast, our method achieves comparable performance with a significantly reduced cumulative total of 120k iterations, facilitated by uniform sampling across the four tasks, resulting in an approximate 50% reduction in the number of iterations. Thus, this streamlined approach markedly reduces the overall computational resource requirements and highlights our practical advantages over conventional learning-based methods.

Inference on unseen task. When handling unseen/out-of-distribution data, UniReg requires the input of anatomical regions and inter/intra-properties. In Table 3, we have performed this evaluation, i.e., we examine the registration of lung tumor, *one completely unseen anatomy*, and our conditioning vector was defined as chest & intra. All learning-based task-specific models (PIVIT, SAME, etc.) failed, as

Organ Name	B. λ	B. Dice	M. λ	M. Dice
Spleen	0.6	73.06	0.5	72.88
R kidney	0.1	71.58		71.05
L kidney	0.5	74.89		74.89
Gall bladder	0.5	42.05		42.05
Esophagus	0.5	42.99		42.99
Liver	0.6	80.13		80.00
Stomach	0.6	34.09		33.55
Aorta	0.2	73.16		72.59
Vena cava	0.6	70.36		70.29
Vein	0.5	31.21		31.21
Pancreas	0.6	27.00		26.82
L adrenal	0.6	30.82		30.58
R adrenal	0.6	28.58		28.44
Mean	—	52.30	—	52.10

Table 4. Regularization priors for 13 different organs in abdominal data. The B. λ represents the best hyperparameters for the specific organ, while M. λ denotes the best hyperparameters for the overall abdomen region. These are obtained using the cLapIRN [34].

indicated by ‘N/A’. Leveraging simple instance optimization (IO), UniReg achieves results that rival those of traditional methods, with a significant advantage of runtime.

4.5. Ablation study

How to define task ID? Why do we categorize tasks according to the head, neck, and chest regions rather than adopting more specific designations for individual organs? As demonstrated in Table 4, our analysis indicates that, while distinct abdominal organs possess unique hyperparameter configurations, the average optimal hyperparameters across all 13 organs produce Dice scores that are comparable to those achieved at the individual organ level. Consequently, we do not employ more precise organ-specific

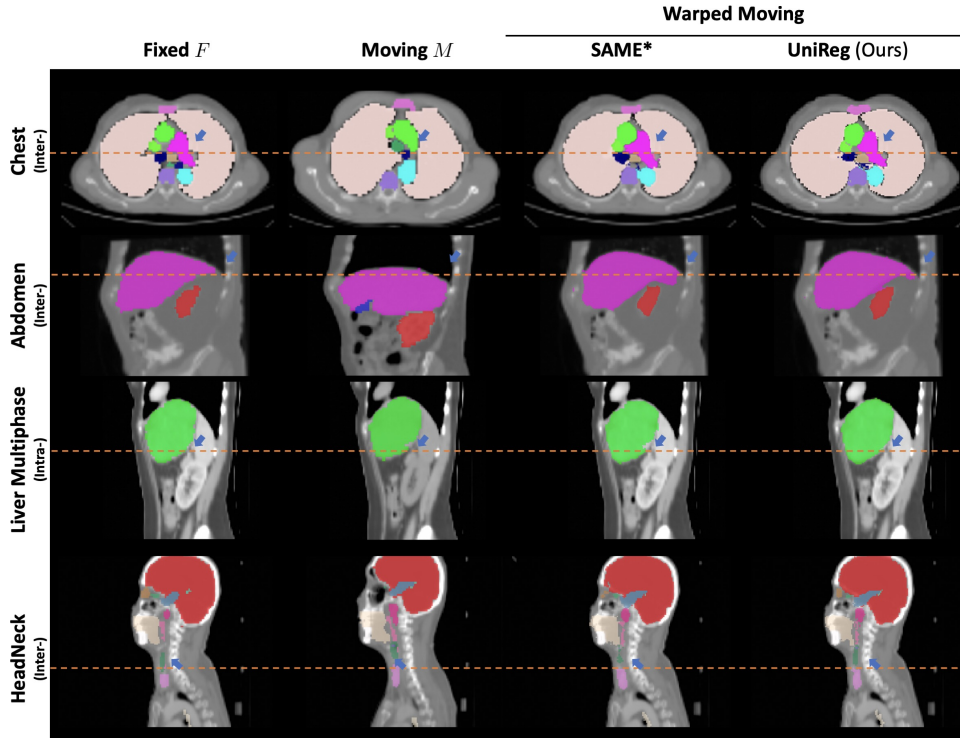


Figure 3. Example slices of top two registration methods. The warped anatomical segmentations are overlaid and major registration artifacts are highlighted with blue arrows. SAME* denotes the semi-supervised SAME model. *Chest*: *A.ascendens*, *A.descendens*, *A.pulmonary*, *A.vertebral.R*, *Bronchus*, *R*, *Lung*, *L*, *Spine*, *Sternum*, *Trachea*, *V.subclavian R*. *Abdomen*: *liver* and *spleen*. *Multiphase CT*: *tumor*. *HeadNeck*: *Brain*, *ETbone L*, *Eye L*, *Hippocampus L*, *IAC R*, *MiddleEar R*, *OpticNerve R*, *Pharynx*, *Thyroid*, *TympanicCavity L*.

UniReg Variants	Abdomen		Liver	
	DSC ₁₃ ↑	SDlogJ ↓	DSC ₂ ↑	SDlogJ ↓
w/ Abdomen Task ID	55.56	1.39	84.66	7.48
w/ Liver Task ID	55.10	1.22	86.42	3.20

Table 5. Influence of the Task ID on registration.

designations in this work. Additionally, in Table 5, we conducted an ablation analysis of the significance of task ID encoding, indicating that the model could not achieve optimal results without correct task IDs.

Condition analysis. The kernels of the dynamic head are conditioned on both input images and task-specific objectives. A comparative analysis in Table 6 highlights the performance degradation of static models (without dynamic mechanisms) as training progresses, directly linking such decline to misalignment between fixed optimization targets and evolving task requirements. In contrast, our dynamic registration mechanism enables effective simultaneous reconciliation of competing objectives, circumventing performance deterioration while maintaining multidimensional optimization fidelity.

Model	# Iter	Abdomen DSC ₁₃ ↑	Liver DSC ₂ ↑
W/O Dyn. Def. Gen.	10k	42.00	80.82
	40k	40.86	78.36
W/ Dyn. Def. Gen.	10k	49.61	83.87
	40k	54.61	85.41
	80k	55.56	86.42

Table 6. Impact of dynamic deformation generation and the number of iterations on our proposed method.

5. Discussion and Conclusion

Why choose CT imaging? CT is the most dominant imaging modality in radiology and oncology, necessitating precise registration for downstream clinical applications such as diagnosis, treatment planning, and longitudinal monitoring. Its widespread adoption underscores the critical need for reliable alignment. *Transfer to MR modality.* UniReg currently lacks direct applicability for MR registration due to its SAM-based backbone, which is incompatible with MR image. A potential extension involves substituting the SAM features with the learning-free MIND descriptor [15] to enable MR adaptation. We left this as future work.

This paper proposes a dynamic learning framework dedicated to developing a controllable universal registration model on CT imaging. It incorporates general backbone and dynamic deformation estimation, which encodes registration tasks that involve varying anatomical structures, inter- and intra-patient, and body parts. The results using CT data covering 90 distinct organs/tumors demonstrate that the proposed method can be adaptively customized to accommodate a diverse range of registration tasks with comparable performance with contemporary state-of-the-art accuracy and significant computational advantage.

References

- [1] Fakhre Alam, Sami Ur Rahman, Sehat Ullah, and Kamal Gulati. Medical image registration in image guided surgery: Issues, challenges and research opportunities. *Biocybernetics and Biomedical Engineering*, 38(1):71–89, 2018. 1
- [2] John Ashburner. A fast diffeomorphic image registration algorithm. *NeuroImage*, 38(1):95–113, 2007. 6
- [3] Brian B Avants, Nick Tustison, and Gang Song. Advanced normalization tools (ANTs). *Insight j*, 2(365):1–35, 2009. 3
- [4] Brian B Avants, Nicholas J Tustison, Gang Song, Philip A Cook, Arno Klein, and James C Gee. A reproducible evaluation of ants similarity metric performance in brain image registration. *NeuroImage*, 54(3):2033–2044, 2011. 1, 3
- [5] Guha Balakrishnan, Amy Zhao, Mert R Sabuncu, John Guttag, and Adrian V Dalca. Voxelmorph: A learning framework for deformable medical image registration. *IEEE Transactions on Medical Imaging*, 38(8):1788–1800, 2019. 2, 3
- [6] Alexander Bigalke, Lasse Hansen, Tony CW Mok, and Mattias P Heinrich. Unsupervised 3d registration through optimization-guided cyclical self-training. In *International Conference on Medical Image Computing and Computer-Assisted Intervention*, pages 677–687. Springer, 2023. 2
- [7] Junyu Chen, Eric C. Frey, Yufan He, William Paul Segars, Ye Li, and Yong Du. Transmorph: Transformer for unsupervised medical image registration. *Medical Image Anal.*, 82: 102615, 2022. 3
- [8] Neel Dey, Mengwei Ren, Adrian V. Dalca, and Guido Gerig. Generative adversarial registration for improved conditional deformable templates. In *2021 IEEE/CVF International Conference on Computer Vision, ICCV 2021, Montreal, QC, Canada, October 10-17, 2021*, pages 3909–3921. IEEE, 2021. 2
- [9] Lee R Dice. Measures of the amount of ecologic association between species. *Ecology*, 26(3):297–302, 1945. 6
- [10] Muthuveni Ezhil, Sastry Vadam, Peter Balter, Bum Choi, Dragan Mirkovic, George Starkschall, and Joe Y Chang. Determination of patient-specific internal gross tumor volumes for lung cancer using four-dimensional computed tomography. *Radiation oncology*, 4:1–14, 2009. 1
- [11] Xin Fan, Zi Li, Ziyang Li, Xiaolin Wang, Risheng Liu, Zhongxuan Luo, and Hao Huang. Automated learning for deformable medical image registration by jointly optimizing network architectures and objective functions. *IEEE Trans. Image Process.*, 32:4880–4892, 2023. 3
- [12] Dazhou Guo, Xianghua Ye, Jia Ge, Xing Di, Le Lu, Lingyun Huang, Guotong Xie, Jing Xiao, Zhongjie Lu, Ling Peng, et al. Deepstationing: thoracic lymph node station parsing in ct scans using anatomical context encoding and key organ auto-search. In *Medical Image Computing and Computer Assisted Intervention*, pages 3–12. Springer, 2021. 5
- [13] David Ha, Andrew Dai, and Quoc V Le. Hypernetworks. *arXiv preprint arXiv:1609.09106*, 2016. 3
- [14] Mattias P. Heinrich, Mark Jenkinson, Michael Brady, and Julia A. Schnabel. Globally optimal deformable registration on a minimum spanning tree using dense displacement sampling. In *Medical Image Computing and Computer Assisted Intervention*, pages 115–122, 2012. 1, 3, 6, 7
- [15] Mattias P Heinrich, Mark Jenkinson, Bartłomiej W Papież, Sir Michael Brady, and Julia A Schnabel. Towards realtime multimodal fusion for image-guided interventions using self-similarities. In *Medical Image Computing and Computer-Assisted Intervention*, pages 187–194, 2013. 3, 8
- [16] Malte Hoffmann, Benjamin Billot, Douglas N Greve, Juan Eugenio Iglesias, Bruce Fischl, and Adrian V Dalca. Synthmorph: learning contrast-invariant registration without acquired images. *IEEE transactions on medical imaging*, 41(3):543–558, 2021. 3
- [17] Andrew Hoopes, Malte Hoffmann, Bruce Fischl, John Guttag, and Adrian V Dalca. Hypermorph: Amortized hyperparameter learning for image registration. In *Information Processing in Medical Imaging: 27th International Conference, IPMI 2021, Virtual Event, June 28–June 30, 2021, Proceedings 27*, pages 3–17. Springer, 2021. 2, 3, 5
- [18] Xun Huang and Serge Belongie. Arbitrary style transfer in real-time with adaptive instance normalization. In *Proceedings of the IEEE international conference on computer vision*, pages 1501–1510, 2017. 3
- [19] Max Jaderberg, Karen Simonyan, Andrew Zisserman, and Koray Kavukcuoglu. Spatial transformer networks. In *Annual Conference on Neural Information Processing Systems*, pages 2017–2025, 2015. 5
- [20] Xu Jia, Bert De Brabandere, Tinne Tuytelaars, and Luc V Gool. Dynamic filter networks. *Advances in neural information processing systems*, 29, 2016. 3, 5
- [21] Philipp Krähenbühl and Vladlen Koltun. Efficient inference in fully connected crfs with gaussian edge potentials. In *Advances in Neural Information Processing Systems*, pages 109–117, 2011. 5
- [22] Ziyang Li, Zi Li, Risheng Liu, Zhongxuan Luo, and Xin Fan. Coupling deep deformable registration with contextual refinement for semi-supervised medical image segmentation. In *19th IEEE International Symposium on Biomedical Imaging, ISBI*, pages 1–5, 2022. 1
- [23] Zi Li, Lin Tian, Tony C. W. Mok, Xiaoyu Bai, Puyang Wang, Jia Ge, Jingren Zhou, Le Lu, Xianghua Ye, Ke Yan, and Dakai Jin. Samconvex: Fast discrete optimization for CT registration using self-supervised anatomical embedding and correlation pyramid. In *Medical Image Computing and Computer Assisted Intervention*, pages 559–569, 2023. 2, 3, 4

- [24] Fengze Liu, Jinzheng Cai, Yuankai Huo, Chi-Tung Cheng, Ashwin Raju, Dakai Jin, Jing Xiao, Alan L. Yuille, Le Lu, Chien-Hung Liao, and Adam P. Harrison. JSSR: A joint synthesis, segmentation, and registration system for 3d multi-modal image alignment of large-scale pathological CT scans. In *ECCV*, pages 257–274. Springer, 2020. 3
- [25] Fengze Liu, Ke Yan, Adam P. Harrison, Dazhou Guo, Le Lu, Alan L. Yuille, Lingyun Huang, Guotong Xie, Jing Xiao, Xi-anhua Ye, and Dakai Jin. SAME: deformable image registration based on self-supervised anatomical embeddings. In *Medical Image Computing and Computer Assisted Intervention*, pages 87–97, 2021. 2, 3, 4
- [26] Risheng Liu, Zi Li, Yuxi Zhang, Xin Fan, and Zhongxuan Luo. Bi-level probabilistic feature learning for deformable image registration. In *Proceedings of the Twenty-Ninth International Joint Conference on Artificial Intelligence, IJCAI*, pages 723–730. ijcai.org, 2020. 3
- [27] Risheng Liu, Zi Li, Xin Fan, Chenying Zhao, Hao Huang, and Zhongxuan Luo. Learning deformable image registration from optimization: Perspective, modules, bilevel training and beyond. *IEEE Transactions on Pattern Analysis Machine Intelligence*, 44(11):7688–7704, 2022. 2, 3, 5
- [28] Tai Ma, Xinru Dai, Suwei Zhang, and Ying Wen. Pivit: Large deformation image registration with pyramid-iterative vision transformer. In *International Conference on Medical Image Computing and Computer-Assisted Intervention*, pages 602–612. Springer, 2023. 3
- [29] Tai Ma, Suwei Zhang, Jiafeng Li, and Ying Wen. Iirp-net: Iterative inference residual pyramid network for enhanced image registration. In *Proceedings of the IEEE/CVF Conference on Computer Vision and Pattern Recognition*, pages 11546–11555, 2024. 2, 6, 7, 1
- [30] Calvin R Maurer and J Michael Fitzpatrick. A review of medical image registration. *Interactive image-guided neurosurgery*, 1:17–44, 1993. 1
- [31] Mingyuan Meng, Lei Bi, Dagan Feng, and Jinman Kim. Non-iterative coarse-to-fine registration based on single-pass deep cumulative learning. In *International Conference on Medical Image Computing and Computer-Assisted Intervention*, pages 88–97. Springer, 2022. 2
- [32] Mingyuan Meng, Dagan Feng, Lei Bi, and Jinman Kim. Correlation-aware coarse-to-fine mlps for deformable medical image registration. In *Proceedings of the IEEE/CVF Conference on Computer Vision and Pattern Recognition*, pages 9645–9654, 2024. 2, 6, 7, 1
- [33] Tony CW Mok and Albert Chung. Fast symmetric diffeomorphic image registration with convolutional neural networks. In *Proceedings of the IEEE/CVF conference on computer vision and pattern recognition*, pages 4644–4653, 2020. 3
- [34] Tony CW Mok and Albert CS Chung. Conditional deformable image registration with convolutional neural network. In *Medical Image Computing and Computer Assisted Intervention–MICCAI 2021: 24th International Conference, Strasbourg, France, September 27–October 1, 2021, Proceedings, Part IV 24*, pages 35–45. Springer, 2021. 2, 3, 5, 7
- [35] Tony CW Mok and Albert CS Chung. Unsupervised deformable image registration with absent correspondences in pre-operative and post-recurrence brain tumor mri scans. In *International Conference on Medical Image Computing and Computer-Assisted Intervention*, pages 25–35. Springer, 2022. 1, 3
- [36] Tony CW Mok, Zi Li, Yingda Xia, Jiawen Yao, Ling Zhang, Jingren Zhou, and Le Lu. Deformable medical image registration under distribution shifts with neural instance optimization. In *International Workshop on Machine Learning in Medical Imaging*, pages 126–136. Springer, 2023. 3
- [37] Tony CW Mok, Zi Li, Yunhao Bai, Jianpeng Zhang, Wei Liu, Yan-Jie Zhou, Ke Yan, Dakai Jin, Yu Shi, Xiaoli Yin, et al. Modality-agnostic structural image representation learning for deformable multi-modality medical image registration. In *Proceedings of the IEEE/CVF Conference on Computer Vision and Pattern Recognition*, pages 11215–11225, 2024. 2, 3
- [38] Tony C. W. Mok and Albert C. S. Chung. Large deformation diffeomorphic image registration with laplacian pyramid networks. In *Medical Image Computing and Computer Assisted Intervention*, pages 211–221, 2020. 2, 3, 6, 7, 1
- [39] Josien PW Pluim, JB Antoine Maintz, and Max A Viergever. Image registration by maximization of combined mutual information and gradient information. In *Medical Image Computing and Computer-Assisted Intervention–MICCAI 2000: Third International Conference, Pittsburgh, PA, USA, October 11–14, 2000. Proceedings 3*, pages 452–461. Springer, 2000. 1, 3
- [40] Chen Qin, Wenjia Bai, Jo Schlemper, Steffen E. Petersen, Stefan K. Piechnik, Stefan Neubauer, and Daniel Rueckert. Joint learning of motion estimation and segmentation for cardiac MR image sequences. In *Medical Image Computing and Computer Assisted Intervention - MICCAI*, pages 472–480. Springer, 2018. 1
- [41] Dinggang Shen and Christos Davatzikos. Hammer: hierarchical attribute matching mechanism for elastic registration. *IEEE Transactions on medical imaging*, 21(11):1421–1439, 2002. 1, 3
- [42] Hanna Siebert, Christoph Großbröhmer, Lasse Hansen, and Mattias P Heinrich. Convexadam: Self-configuring dual-optimisation-based 3d multitask medical image registration. *IEEE Transactions on Medical Imaging*, 2024. 3
- [43] Aristeidis Sotiras, Christos Davatzikos, and Nikos Paragios. Deformable medical image registration: A survey. *IEEE Transactions on Medical Imaging*, 32(7):1153–1190, 2013. 1
- [44] Wei Sun, Wiro J Niessen, and Stefan Klein. Free-form deformation using lower-order b-spline for nonrigid image registration. In *Medical Image Computing and Computer Assisted Intervention*, pages 194–201, 2014. 1, 3, 6, 7
- [45] Lin Tian, Zi Li, Fengze Liu, Xiaoyu Bai, Jia Ge, Le Lu, Marc Niethammer, Xianghua Ye, Ke Yan, and Dakai Jin. SAME++: A self-supervised anatomical embeddings enhanced medical image registration framework using stable sampling and regularized transformation. *CoRR*, abs/2311.14986, 2023. 3, 4, 6, 7, 1

- [46] Lin Tian, Thomas Hastings Greer, Roland Kwitt, François-Xavier Vialard, Raúl San José Estépar, Sylvain Bouix, Richard J. Rushmore, and Marc Niethammer. unigradicon: A foundation model for medical image registration. In *Medical Image Computing and Computer Assisted Intervention - MICCAI 2024 - 27th International Conference, Marrakesh, Morocco, October 6-10, 2024, Proceedings, Part II*, pages 749–760. Springer, 2024. 2, 3, 6, 7, 1
- [47] Zhenlin Xu and Marc Niethammer. Deepatlas: Joint semi-supervised learning of image registration and segmentation. In *Medical Image Computing and Computer Assisted Intervention*, pages 420–429, 2019. 3
- [48] Ke Yan, Le Lu, and Ronald M. Summers. Unsupervised body part regression via spatially self-ordering convolutional neural networks. In *15th IEEE International Symposium on Biomedical Imaging, ISBI*, pages 1022–1025. IEEE, 2018. 6
- [49] Ke Yan, Jinzheng Cai, Dakai Jin, Shun Miao, Dazhou Guo, Adam P Harrison, Youbao Tang, Jing Xiao, Jingjing Lu, and Le Lu. Sam: Self-supervised learning of pixel-wise anatomical embeddings in radiological images. *IEEE Transactions on Medical Imaging*, 2022. 3, 4
- [50] Jianpeng Zhang, Yutong Xie, Yong Xia, and Chunhua Shen. Dodnet: Learning to segment multi-organ and tumors from multiple partially labeled datasets. In *Proceedings of the IEEE/CVF conference on computer vision and pattern recognition*, pages 1195–1204, 2021. 3, 5
- [51] Amy Zhao, Guha Balakrishnan, Frédo Durand, John V. Guttag, and Adrian V. Dalca. Data augmentation using learned transformations for one-shot medical image segmentation. In *IEEE Conference on Computer Vision and Pattern Recognition, CVPR*, pages 8543–8553, 2019. 1
- [52] Shengyu Zhao, Yue Dong, Eric I-Chao Chang, and Yan Xu. Recursive cascaded networks for unsupervised medical image registration. In *2019 IEEE/CVF International Conference on Computer Vision, ICCV 2019, Seoul, Korea (South), October 27 - November 2, 2019*, pages 10599–10609. IEEE, 2019. 3

UniReg: Foundation Model for Controllable Medical Image Registration

Supplementary Material

A. Network Architecture

Figure 4 illustrates the network architecture of the shared backbone. Table 7 depicts the variables employed within this shared backbone, with fixed image F and moving image M serving as representative examples.

Variables	Tensor Shape
Image Tensor F	$(B, 2, D, W, H)$
SAM Fine Feature of F	$(B, 128, D/2, W/2, H/2)$
SAM Coarse Feature of F	$(B, 128, D/4, W/16, H/16)$
Image Tensor M	$(B, 2, D, W, H)$
SAM Fine Feature of M	$(B, 128, D/2, W/2, H/2)$
SAM Coarse Feature of M	$(B, 128, D/4, W/16, H/16)$
SAM CorrLayer of F, M	$(B, 27, D/2, W/2, H/2)$

Table 7. Shape of variables used in shared backbone. H , W and D refer to the input volume’s height, width and depth. The first channel of F or M is for SAM extraction and the second is for the shared backbone network.

B. Details of Datasets

HeadNeck. The dataset includes annotations for 45 head and neck organs, specifically: Brain, Brainstem, Chiasm, L. Cochlea, R. Cochlea, Esophagus, L. Eustachian Tube, R. Eustachian Tube, L. Eye, R. Eye, L. Hippocampus, R. Hippocampus, L. Internal Auditory Canal, R. Internal Auditory Canal, Larynx, Glottic Larynx, Supraglottic Larynx, L. Lens, R. Lens, L. Mandible, R. Mandible, L. Mastoid, R. Mastoid, L. Middle Ear, R. Middle Ear, L. Optic Nerve, R. Optic Nerve, Oral Cavity, L. Parotid, R. Parotid, Pharyngeal Constrictor Muscle, Pituitary Gland, Spinal Cord, L. Submandibular Gland, R. Submandibular Gland, L. Temporal Lobe, R. Temporal Lobe, Thyroid, L. Temporomandibular Joint, R. Temporomandibular Joint, Trachea, L. Tympanic Cavity, R. Tympanic Cavity, L. Vestibular Semicircular Canal, and R. Vestibular Semicircular Canal.

Chest. Each chest CT image features 35 manually labeled anatomical structures identified by a senior radiologist, including: Sternum, Spine, A.CCA.L, A.CCA.R, A.Pulmonary, A.Subclavian.L, A.Subclavian.R, A.Vertebra.L, A.Vertebra.R, V.Azygos, V.BCV.L, V.BCV.R, V.IJV.L, V.IJV.R, V.IVC, V.Pulmonary, V.Subclavian.L, V.Subclavian.R, V.SVC, Thyroid. L, Thyroid. R, M.Anterior.Cervi, M.Scalenus, M.Scalenus.A, M.Scleido, A.Arch, A.Ascendens, A.Descendens, Trachea, A.Bronchus.L, A.Bronchus.R, Lung. L, Lung. R, Eso, and Heart.

Abdomen. The Abdomen CT dataset from Learn2Reg³ includes 30 abdominal scans, each containing 13 manually labeled anatomical structures: spleen, right kidney, left kidney, gallbladder, esophagus, liver, stomach, aorta, inferior vena cava, portal vein, splenic vein, pancreas, left adrenal gland, and right adrenal gland.

C. Details of Baselines

We compare with conventional methods (NiftyReg⁴ [44], Deeds⁵ [14], and state-of-the-art learning-based approaches (LapIRN⁶ [38], SAME⁷ [45], IIRP-Net⁸ [29], CorrMLP⁹ [32], and (uniGradICON¹⁰ [46]).

The command and parameters we used for *NiftyReg* [44]:

```
reg_f3d -ref [<Fixed>] -flo [<Moving>]
-cpp <OutFileSpec> -res <OutWarpedFile>
```

The command and parameters we used for *Deeds* [14]:

```
deedsBCV -F [<Fixed>] -M [<Moving>]
-O <OutFileSpec> -S <InSegmentationFile>
```

Learning-based baselines. The learning-based methods LapIRN, IIRP-Net, CorrMLP, and SAME are trained from scratch on four datasets, with the number of optimization iterations set to 80,000 for each task, and the learning rate set to $5e - 5$. Note that, our UniReg employs a random sampling approach from four distinct tasks and executes 120,000 optimization iterations across these tasks in total. For SAME, we employ the same loss functions—namely, Normalized Cross-Correlation (NCC), Dice coefficient, and diffusion regularizer—as well as the same hyperparameter settings utilized in UniReg, as detailed in Table 8. For the remaining two methods, we adopt the loss functions and recommended hyperparameter combinations provided by the original repository. All learning-based approaches, including the method proposed in this study, are configured to utilize a batch size of 1.

UniGradICON. UniGradICON serves as a foundational model for diffeomorphic registration and has undergone training on diverse datasets. In this study, we employ the pre-existing binaries made available in their repository, opting not to conduct any retraining.

³<https://learn2reg.grand-challenge.org/Learn2Reg2020/>

⁴<http://cmictg.cs.ucl.ac.uk/wiki/index.php/NiftyReg>

⁵<https://github.com/mattiaspaul/deedsBCV>

⁶<https://github.com/cwmok/LapIRN>

⁷<https://github.com/alibaba-damo-academy/same>

⁸<https://github.com/Torbjorn1997/IIRP-Net>

⁹<https://github.com/MungoMeng/Registration-CorrMLP>

¹⁰<https://github.com/uncbiag/uniGradICON>

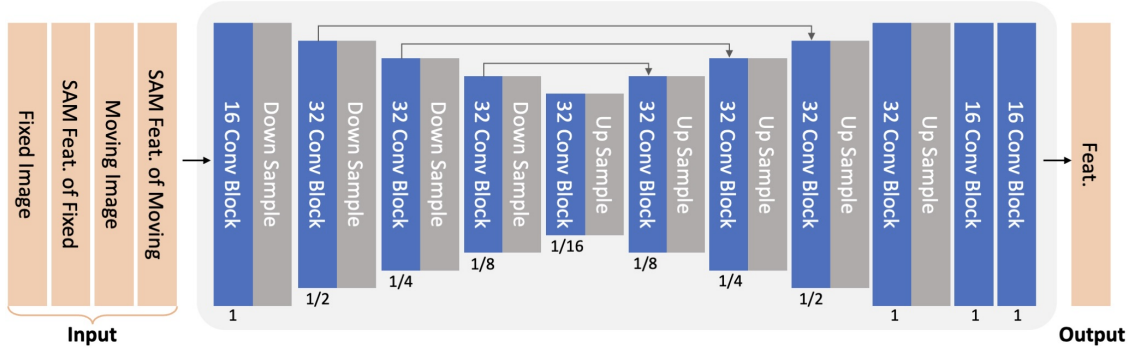


Figure 4. Network Architecture of the Shared Backbone. Each blue rectangle represents a convolutional layer, with the number of channels indicated within the rectangle and the spatial resolution relative to the input volume displayed below. Following each convolutional layer, the LeakReLU activation function is applied.

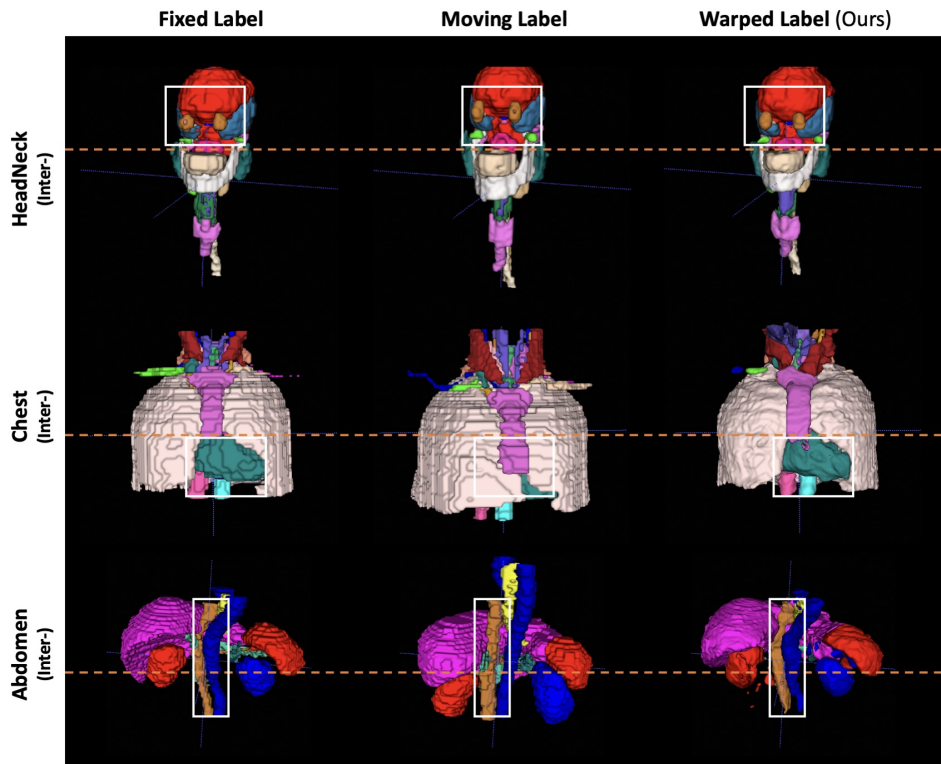


Figure 5. Examples of three-dimensional rendering volume maps derived from the warped segmentation images of the HeadNeck, Chest, and Abdomen tasks. The highlighted white boxes delineate the regions in which our UniReg attains precise alignment.

Regularization Priors	HeadNeck λ	Chest λ	Abdomen λ	Liver λ
Hyperparameter value	0.05	1	0.1	10

three-dimensional volumetric renderings derived from the warped segmentation.

Table 8. Hyperparameters used in the training process on the HeadNeck, Chest, Abdomen and Liver registration tasks.

D. Additional Experimental Results

Visualization. To further illustrate the variations in registration results of anatomical structures, Figure 5 presents